Nanoscale

Accepted Manuscript

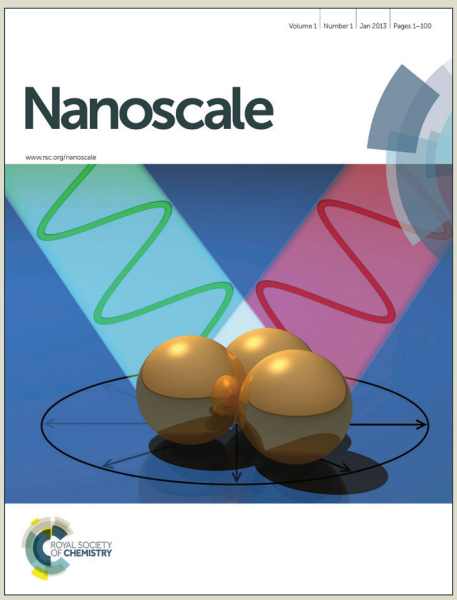

ROYAL SOCIETY OF CHEMISTRY

www.rsc.org/nanoscale

Nanoscale

RSCPublishing

COMMUNICATION

Hierarchical construction of a mechanically stable peptide-graphene oxide hybrid hydrogel for drug delivery and pulsatile triggered release *in vivo*†

Cite this: DOI: 10.1039/x0xx00000x

Received 00th January 2012,
Accepted 00th January 2012

DOI: 10.1039/x0xx00000x

www.rsc.org/

Junhua Wu[a,b], Aiping Chen[b], Meng Qin[a], Rong Huang[b], Guang Zhang[c], Bin Xue[a], Xiang Gao[a], Ying Li*[d], Yi Cao*[a] and Wei Wang*[a]

Design hydrogels with controllable drug-release properties remains challenging. Here we report a hydrogel made of hierarchical graphene oxide sheets and peptide assemblies for on-demand drug release. The hydrogel possesses high drug-sustainability and the release of drugs can be precisely and remotely controlled through external stimuli.

Hydrogels have been extensively explored as promising biomaterials for biosensor,[1-3] tissue engineering,[4-6] and drug delivery,[7-12] because of their great biocompatibility, environmental responsiveness, and tunable mechanical and bioactive properties mimicking the natural extracellular matrices.[13-15] For drug delivery, supramolecular hydrogels may be advantageous over polymeric ones, because they are often injectable and can be precisely delivered to the lesion.[11, 16-23] However, many supramolecular hydrogels are of low mechanical stability and high erosion rates, and therefore are unstable *in vivo*.[24-28] This greatly hinders the application of supramolecular hydrogels for drug delivery and controlled release. On the other hand, the release of drugs from the hydrogel matrix is typically through the physical diffusion or gradual decomposition of the hydrogel.[29] It is difficult to regulate the drug release in a predictable fashion and on-demand.[30-32] Especially, examples of drug delivery system that can perform both "on" and "off" switch for drug release are scarce. Hence, it is highly desirable to formulate new types of hydrogels that can overcome these limitations for efficient drug delivery. To this end, here we report a hierarchical construction approach for novel peptide-graphene hybrid hydrogels that combines properties such as high mechanical stability, syringe-injectability, low erosion rate, and near-infrared light triggered release functionalities. The hydrogel possesses high drug-sustainability and the release of drugs only occurs in the presence of external stimuli. These allow to precisely and remotely controlling the dose of drugs in the lesion. We anticipate such hydrogels can find broad applications in drug delivery.

The design of this peptide-graphene hybrid hydrogel is depicted in Fig. 1. The peptide contains a graphene binding motif (pyrene) [33-35] at the N-terminus, a glycine-alanine (GA) repeat sequence derived from *Bombyx mori* silk at the center, capable of forming antiparallel β sheets in solution,[36, 37] and a tyrosine residue at the C-terminus, which can be photo-crosslinked by a ruthenium catalyzed reaction.[38, 39] The peptide is named as PyGAGAGY hereafter. Owing to strong π-π stacking between pyrene and graphene, the peptides can be non-covalently linked to the surface of graphene oxide sheets (GOS). Subsequently, the formation of β sheets between GA repeats facilitates the inter-sheet crosslinking among various GOS. Further photo-crosslinking of the terminal tyrosine motif leads to the formation of strong hydrogels. In such a design, different types of interactions of hierarchical strength were entailed in the hybrid hydrogel. The covalent crosslinks (i.e. dityrosine adducts) serve as permanent joints, imparting high stability, whereas weak bonds (e.g. hydrophobic interactions between pyrene and GOS, and hydrogen bonds among GA repeats) are environmental sensitive and can be used for triggered drug release. Moreover, GOS is well-known for its photo-thermal property due to its near-infrared (NIR) absorption ability.[40-42] The local temperature increase upon NIR irradiation could result in partially unfolding of β sheets formed by GA repeats and weakening of the π-π interactions between pyrene and GOS, triggering the release of encapsulated drugs.

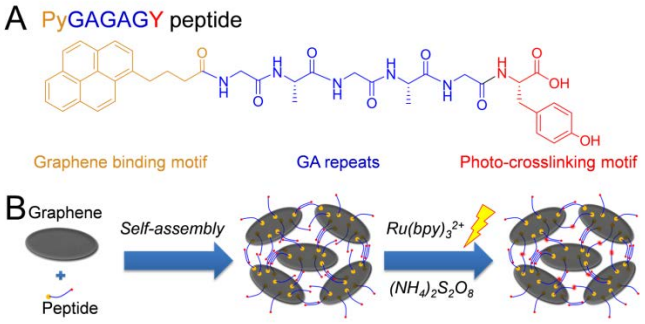

Fig. 1 The design of the hybrid hydrogel. (A) The peptide sequence. (B) The hierarchical construction scheme for the hydrogel.

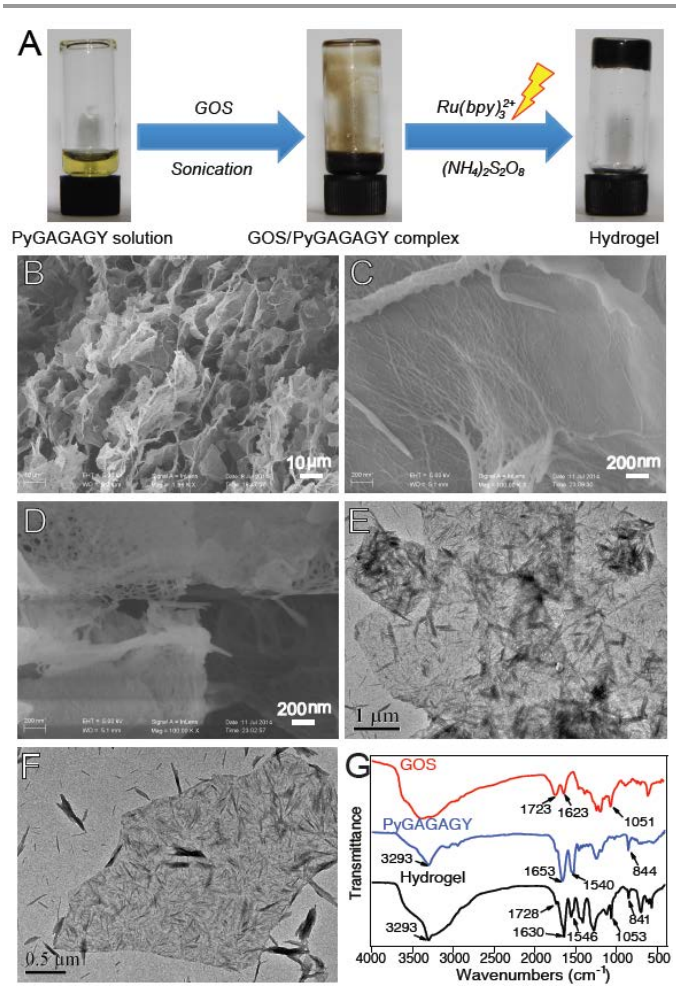

Fig. 2 Structural characterization of the hydrogel. (A) The images for PyGAGAGY solution, dispersed GOS/PyGAGAGY complex and the hydrogel. (B) SEM image of lyophilized hydrogel with low magnification. The diameters of GOS are ~10-20 μm. (C) SEM image of lyophilized hydrogel with high magnification. The surface of GOS is rough due to the presence of peptide layer. The peptide fibers show strong interactions with GOS. (D) Direct view of the interconnected peptide fiber network between graphene layers. (E) TEM image of the hydrogel indicates the hydrogel network is connected by both GOS and peptide fibrils. (F) High magnification TEM image indicates that peptide fibrils are mainly attached to GOS surfaces in the hydrogel. (G) FTIR spectra of GOS, PyGAGAGY, and Hydrogel. Hydrogel shows IR signals from both GOS (1723 nm: ν(C=O); 1623 nm: ν(COO$^-$); 1051 nm: ν(C-O-C)) and the peptide (3293 nm: ν(N-H); 1653 nm: ν(C=O); 1540 nm: δ(N-H); 844 nm: ν(C=C from pyrene)).

We first studied the formation of PyGAGAGY-GOS hybrid hydrogel. The peptide was synthesized using the standard Fmoc-based solid phase method, purified by HPLC, and characterized by mass spectrometry (Fig. S1 and S2). Then the peptide was dissolved in double distilled water (ddH_2O) to make a final concentration of 20 mg mL^{-1} (Fig. 2A). Subsequently, GOS was added into the PyGAGAGY solution and dispersed by sonication for 60 minutes to get a GOS final concentration of 10 mg mL^{-1} (Fig. 2A). PyGAGAGY significantly improved the solubility of GOS by the formation of GOS-peptide complexes, in which the hydrophobic surfaces of GOS were weaved with amphiphilic peptides. Subsequently, $Ru(bpy)_3Cl_2$ (3.0 μL, 1 mM) and ammonium persulfate (APS, 15.0 μL, 600 mM) were added into 300 μL of the GOS dispersed PyGAGAGY solution. The mixture was vigorously vortex-mixed prior to light irradiation. After irradiation with white light (using a Panasonic PT-UX10 projector with a 220-W lamp as the light source) for 1 minute, the dark brown hydrogel was formed (Fig. 2A), due to the formation of dityrosine adducts (Fig. S3). The formation of interconnected porous hydrogel network was confirmed by scanning electron microscope (SEM). As shown in Fig. 2B, the GOS of diameters of ~10-20 μm were densely packed to form the framework of the hydrogel. The surface of GOS was quite rough, which is probably due to the presence of a peptide layer (Fig. 2C). The fibers can tightly attached to the GOS surface through the strong interactions between pyrene and graphene. In the absence of the peptide, the GOS surface was much smoother (Fig. S4). In between GOS layers, the peptide formed interweaved fibrous networks, giving rise to the high integrity and stability of the hydrogel (Fig. 2D). The attachment of peptide fibers to GOS surface in the hydrogel was further confirmed by transmission electron microscope (TEM) (Fig. 2E and 2F). Majority of peptide fibers are attached to GOS instead of being suspended in the hydrogel. The integration of GOS and the peptide in the hydrogel was further confirmed using Fourier transform infrared (FT-IR) spectroscopy (Fig. 2G). The hydrogel samples showed IR signals from both GOS and the peptide. It is worth noting that the structure of this GOS-peptide hybrid hydrogel is distinct from other GOS-peptide hydrogels reported previously.[43, 44] In those hydrogels, peptides self-assemble into fibrils first, and only a small portion interacts with GOS. The major gel backbone is the peptide fibers instead of the graphene-peptide complexes. Therefore, the resulting hydrogel is not mechanically stable enough for triggered-release. In our designed hybrid hydrogel, the peptide alone cannot form hydrogel due to the strong hydrophilicity of the GAGAGY sequence (Fig. 2A and S5). GOS alone and with pre-crosslinked peptides also cannot form hydrogel due to the lack of sufficient peptide-GOS interactions (Fig. S6, S7 and S8). Therefore, the interactions between peptides and GOS are crucial for the formation of the hydrogel and are maximized in this system through increasing the hydrophilicity of the peptide to disfavor inter-peptide interactions. The advantage of such design is that there are multiple parallel connections between various GOS layers. Partially breaking of these interactions will not cause the disassembly of the hydrogel. Therefore, the hydrogel is robust upon external perturbation and suitable for triggered drug release. It is worth mentioning that such a hydrogel design is also advantageous over GOS-drug hybrid hydrogel [45], which is not mechanically strong enough for triggered drug release and may decompose when drug is partially released.

We then tested whether the hydrogel is mechanically stable. We measured the rheological properties of the hydrogel. The storage modulus (G') of the hydrogel is ~0.25 MPa, outperforming many peptide-based supramolecular hydrogels and comparable to many polymeric ones (Fig. 3A).[24, 28, 46] The hydrogel showed a linear viscoelastic region below 5% strain and can be completely destroyed at strains higher than 20% (Fig. S9). We also studied the effect of GOS contents on the mechanical properties of the hybrid hydrogels. It seems that the GOS concentrations of 10-15 mg mL^{-1} are the optimum of the overall mechanical strength of the hydrogel (Fig. S10). Moreover, the hydrogel can quickly reform upon mechanical agitation. As shown in Fig. 3B, we destroyed the hydrogel using a 100% strain and then monitored the recovery of the hydrogel by decreasing the strain back to 1%. The G' can be almost fully

recovered within a few seconds after the mechanical agitation was removed. This provides direct evidence that the hydrogel is suitable for triggered drug release, during which the hydrogel structure may be temporarily destroyed to release the trapped drugs. Moreover, the rapid recovery of the hydrogel upon mechanical agitation makes the hydrogel injectable. As shown in Fig. 3C, the hydrogel can be readily pushed through a syringe tip and quickly reformed after injection (within 5 s). Although the hydrogel is formed mainly through non-covalent interactions, it is quite stable in phosphate buffer saline (PBS, 10 mM). The hydrogel remained intact without significant changes in its shape for at least two months and no measurable erosion of the peptide was detected using UV absorption at 220 nm. The superb stability of the hybrid hydrogel makes it suitable to serve as drug carriers. In order to test the drug releasing property of the hydrogel, we loaded a model anticancer drug, doxorubicin (DOX, 2 mg mL^{-1}) in the hydrogel (Fig. S11 and S12). More than 95% of the drugs in the buffer can be gradually loaded into the hydrogel by simply placing the hydrogel in the drug solution (Fig. S11 and S12). The drug-loaded hydrogel showed extremely slow spontaneous drug release (Fig. 4C). Such strong drug-sustaining ability allows drugs to be stored in the hydrogel for a long period of time without leaking after being delivered to the lesion *in vivo*.

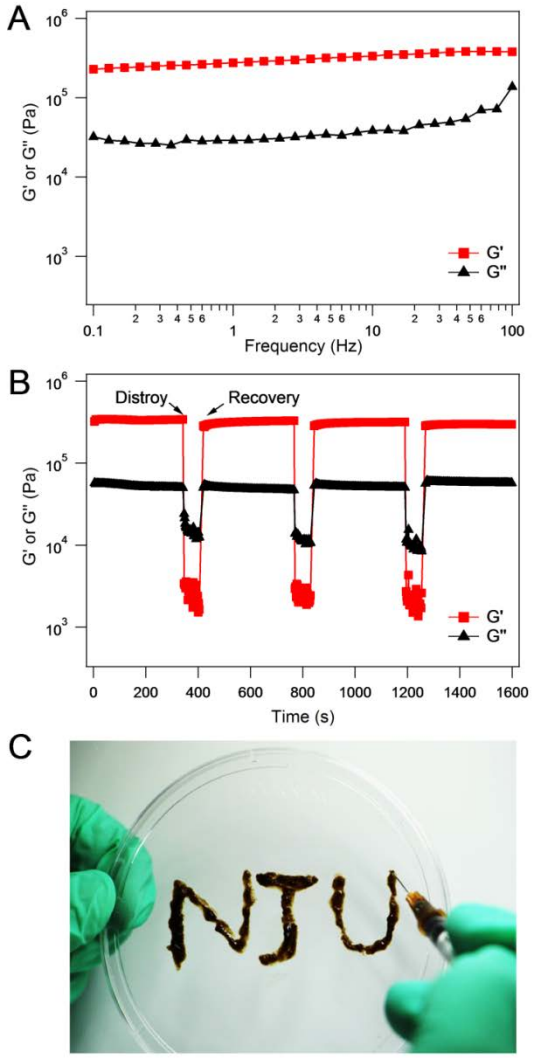

Fig. 3 Mechanical properties of the hybrid hydrogel. (A) The rheological measurement in the dynamic frequency sweep mode for the hydrogel. (B) Three destroy-recovery cycles of the hydrogel. (C) The hydrogel is syringe-injectable and can vertically hang on a petri dish cover without dropping after injection.

Having studied the structure, stability and mechanical properties of the peptide-GOS hybrid hydrogel, we further investigated its triggered drug release properties. As the photo-thermal effects of graphene upon NIR irradiation has been well established (Fig. S13), we measured the NIR irradiation triggered release of DOX from the hydrogel (Fig. 4A). The temperature change of the hybrid hydrogel upon irradiation using an 808-nm laser was studied in detail to find the optimal triggering conditions (Fig. S13). The local temperature of the hydrogel can be adjusted by using different power or different irradiation time. Because the melting temperature of the β sheet structure of PyGAGAGY is ~ 47°C (Fig. 4B), we chose 1.5 W and 2 W for the irradiation. Under these conditions, the β sheet structures can be partially unfolded. The rise of temperature upon NIR irradiation can also disrupt the π-π stacking between pyrene and GOS, which further facilitate the release of drugs. The hydrogel containing 2 mg mL^{-1} of DOX was alternately irradiated using the 808-nm for either 1 min or 2 min at different powers and then stored still for an hour to monitor the drug release (Fig. 4C). DOX showed a burst release upon laser irradiation. The release was terminated once the laser was turned off. Therefore, such triggered release can be applied on-demand. The amount of DOX released each time is also tunable by adjusting the laser power as well as theirradiation time. Moreover, the amount of DOX released after each trigger was proportional to the total amount of DOX remained in the hydrogel and the dose of the drug can be precisely controlled. In the end of the triggered-release experiment, the amount of DOX in the solution and in the gel reached equilibrium. The residual DOX in the hydrogel was estimated to be less than 20%. It is worth noting that the hydrogel remained intact after more than 5 cycles of triggered release (Fig. S14).

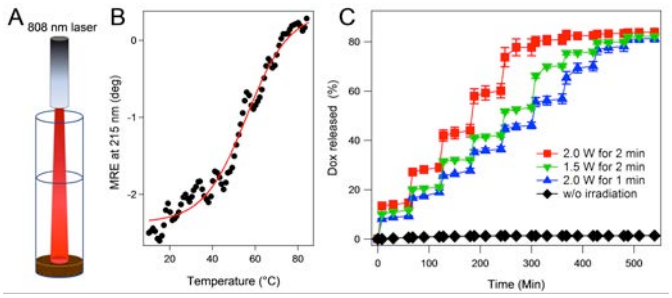

Fig. 4 Triggered-release properties of the hybrid hydrogel. (A) Illustrative scheme of the 808-nm near Infrared laser irradiation triggered release. (B) Thermal melting of PyGAGAGY monitored by circular dichroism. (C) Laser-triggered release of DOX at different laser power and for different time. The laser was turned on every 60 min.

The cytotoxicity of the hydrogel to normal cell lines LO2 was also evaluated. Hydrogels were fractured to millimeter size and suspended in the growth media. Our preliminary data indicated that the hydrogel exhibited high biocompatibility and low cytotoxicity to

normal cell lines (Fig. S15 and S16). As shown in Fig. S17, S18 and S19, both the reactants and the leachable components were safe to the growth of normal cell lines LO2, indicating that the hydrogel is promising for biomedical applications. We further tested the cytotoxicity of the hydrogel to a model cancer cell line, human hepatocarcinoma cell line SMMC-7721, seeded on a 24-well plate on the application of NIR laser irradiation (Fig. 5). The hydrogel alone did not show any appreciable cytotoxicity. The cell morphology also did not change in the presence of DOX-loaded hydrogels. These indicated the low toxicity and great drug sustainability of the hydrogel. Upon NIR irradiation for 2 min, the released DOX could lead to drastic decrease of cell viability (Fig. 5). This is consistent with the *in vitro* drug release experiments.

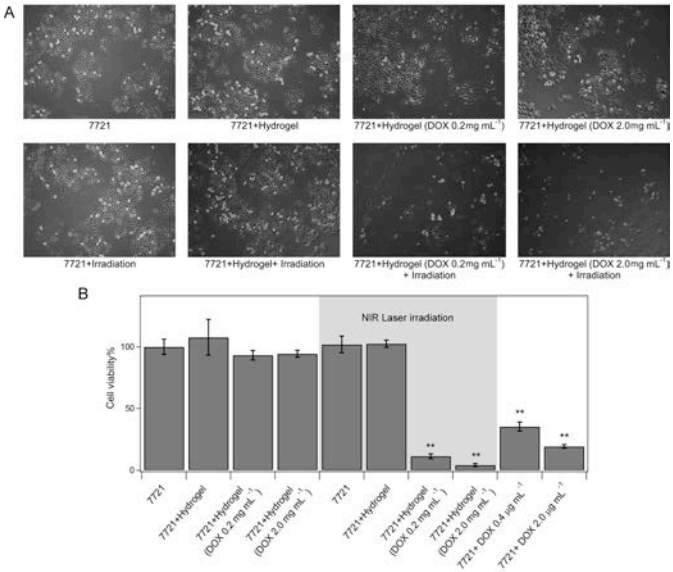

Fig. 5 Laser-triggered cytotoxicity of the DOX-loaded hybrid hydrogel. (A) Photographs of the *hepatocarcinoma* cell line SMMC-7721 grown on a 24-well plate at a density ~1 × 10^4 cells per well in 1.0 mL of DMEM medium (10% FBS, 100U mL^{-1} penicillin, and 100 μg mL^{-1} streptomycin) at 37 °C in a humidified atmosphere containing 5% (v/v) CO_2. After growth for 24 h, 0.1 mL of fractured hydrogel or DOX-loaded hydrogel (containing 0.2 or 2.0 mg mL^{-1} DOX) were added to the desired wells. The irradiation was performed using an 808-nm NIR laser with a spot diameter of ~ 14 mm at 1.5 W for 2 min. All the cells were cultured for additional 4 h and the floating fractured hydrogels were removed by rinsing with DMEM medium before taking the photographs. (B) Cell viability assessed by the MTT method after the photographs were taken. The control group using DOX solution was performed using the same procedure. The final DOX concentrations in the media were 0.4 and 2.0 μg mL^{-1}, respectively. ** indicates $p < 0.01$, compared with 7721 control group.

Ultimately, we evaluated whether the designed hybrid hydrogel is suitable for *in vivo* on-demand anticancer drug release and possesses the antitumor efficiency. Thanks to the thixotropic character, the DOX-loaded hybrid hydrogel can be directly delivered to the desired locations in the nude mice through subcutaneous injection (Fig. 6A). The fluorescence of DOX can be used to monitor the drug release *ex vivo*. Due to the high drug sustainability of the hydrogel, the delivered drug did not show any measurable release in 2 h without external stimuli (Fig. S20A-D). However, upon NIR irradiation, the drug showed burst release and the drug level at the lesion can be retained for at least 2 h (Fig. S20E-H). We also studied the long-term on-demand release of DOX in nude mice. The "on" and "off" switch of DOX release can be repeatedly demonstrated for several cycles (Fig. 6B and S21). The hybrid hydrogel remained stable *in vivo* for at least 13 days after injection. The majority of the released drug can be taken off from the lesion through circulation in ~2-3 days, while the newly released drug triggered by external stimuli can bring back the drug concentration to the original level.

After demonstrating the promising *in vivo* on-demand drug release of the hydrogel, we then investigated the antitumor properties of the DOX-loaded hydrogel. The hydrogels with different amount of loaded DOX were subcutaneously injected near the tumor lesion in the nude mice. DOX-L-gel and DOX-H-gel contain 1.0 and 5.0 mg mL^{-1} DOX, respectively. Apparently, the NIR-triggered on-demand release treatment could efficiently cure the tumor. The tumors in 2 out of 5 treated mice using the DOX-L-gel (DOX-L-gel-irradiation

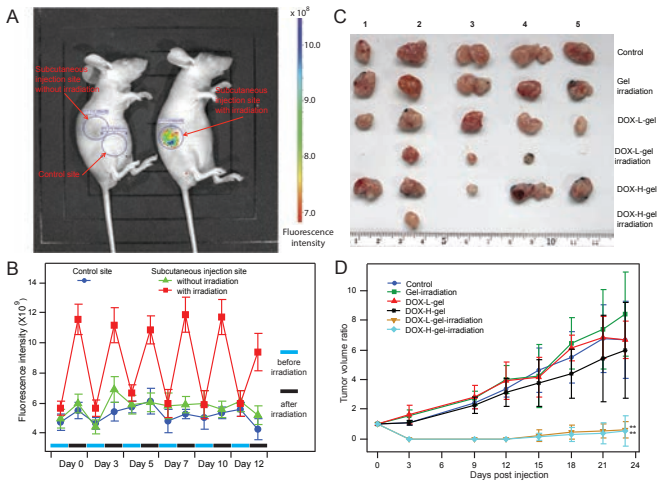

Fig. 6 *In vivo* on-demand drug release and antitumor study. (A) 50 μL of DOX-loaded hydrogel (containing 2 mg mL^{-1} DOX) was subcutaneously injected into two mice. The control site and the subcutaneous injection sites with or without irradiation for on-demand drug release were marked in blue circles in the figure. The fluorescence of DOX (excitation at 465 nm and emission at 570 nm) was used to monitor the drug release by imaging analysis. The on-demand DOX release was triggered by irradiating the raised skin caused by subcutaneous injection with an 808-nm near infrared laser at 2.0 W for 1 min. (B) The fluorescence intensities of the subcutaneous injection site before and after irradiation in different days (red square). The fluorescence intensities of the subcutaneous injection site without irradiation (green triangle) and the control site upon irradiation (blue circle) were also shown for comparison. (C) The image of tumors taken from 6 groups of sacrificed mice at day 23 (5 mice/group). In this experiment, tumor-bearing mice were injected by 50 μL of hydrogel containing 1.0 or 5.0 mg mL^{-1} of DOX with (labeling as DOX-L-gel-irradiation and DOX-H-gel-irradiation, respectively) or without irradiation (labeling as DOX-L-gel and DOX-H-gel, respectively). The mice without treatment (Control group) and that treated with DOX unloaded hydrogel (Gel-irradiation group) were also studied. In the DOX-L-gel-irradiation group, two mice had been cured and had no tumor, and in the DOX-H-gel-irradiation group, four mice had been cured and had no tumor. (D) The size of the tumors during the treatment. (**indicates $p < 0.01$, compared with control group.)

group) and 4 out of 5 treated mice using the DOX-H-gel (DOX-H-gel-irradiation group) were disappeared after a course of treatment of 23 days (Fig. 6C). Moreover, the tumor size of the un-irradiated mice (DOX-L-gel and DOX-H-gel group) showed similar tumor size as the control group and the mice treated by DOX unloaded hydrogel (Gel-irradiation group), indicating that the anti-tumor efficiency of the hydrogel is through the on-demand release of the loaded drug instead of drug leaking due to the decomposition of the hydrogel. The weight of the tumor taken from sacrificed mice was summarized

in Fig. S22. The size of the tumor in different groups during the course of treatment were shown in Fig. 6D. The growth of the tumor in the NIR irradiated groups only took place after 15 days post injection (10 days post last irradiation). It is apparently possible to raise the drug concentration through additional irradiation at day 15 to further improve the antitumor efficiency of the treatment. The beauty of the on-demand release system is its ability to actively control the drug level to achieve the optimum treatment while minimize the side effects of high dose.

Conclusions

In summary, we reported a peptide-graphene hybrid hydrogel for drug delivery and pulse-triggered release. The hydrogel is composed of graphene oxide sheets interconnected by hierarchical peptide interactions. The peptide and graphene are linked by π-π interactions and the peptide molecules are connected either by hydrogen bonds in the antiparallel β sheets or by direct covalent crosslinking. The strong interactions serve as permanent crosslinks that warrant the high stability of the hydrogel whereas the weak interactions could be temporarily broken upon external triggering. Such a design make the hydrogel mechanically and chemically stable, injectable, and suitable for being triggered by NIR irradiation. Moreover, the hydrogel exhibits low cytotoxicity and can be used *in vivo*. With these excellent traits, we anticipate that this type of hybrid hydrogels has high potential for broad biomedical applications.

Acknowledgements

We thank Prof. Huaiping Cong for her kind help on SEM measurements. This work was supported by the National Natural Science Foundation of China (Grant Nos. 11304156, 11334004, 91127026, 31170813, 30801417 and 81172143), China Postdoctoral Science Foundation (Grant No. 2013M531312), the Natural Science Foundation of Jiangsu Province (Grant No. BK20141324), the Scientific Research Foundation for the Returned Overseas Chinese Scholars (State Education Ministry, China), the Start-up research fund of NUIST, the Priority Academic Program Development of Jiangsu Higher Education Institutions, and the startup funding of NUIST.

Notes and references

[a] National Laboratory of Solid State Microstructure, Department of Physics, Nanjing University, 22 Hankou Road, Nanjing, Jiangsu, China 210093; Email: caoyi@nju.edu.cn; wangwei@nju.edu.cn

[b] Medical School, Nanjing University, 22 Hankou Road, Nanjing, Jiangsu, China 210093

[c] Affiliated Drum Tower Hospital, Gulou School of Clinical Medicine, Nanjing Medical University, Nanjing, Jiangsu, China 210046

[d] Address here. Jiangsu Key Laboratory of Atmospheric Environment Monitoring & Pollution Control, Chemistry Department, School of Environmental Science & Engineering, Nanjing University of Information Science & Technology, 219 Ningliu Road, Nanjing, Jiangsu, China 210044; Email: yingliubc@gmail.com

† Electronic Supplementary Information (ESI) available: [Detailed experimental procedures and supporting figures]. See DOI: 10.1039/c000000x/

1. G. R. Hendrickson and L. Andrew Lyon, *Soft Matter*, 2009, 5, 29-35.
2. C. Ren, H. Wang, X. Zhang, D. Ding, L. Wang and Z. Yang, *Chem. Commun. (Cambridge, U. K.)*, 2014, 50, 3473-3475.
3. H. Wang, J. Liu, A. Han, N. Xiao, Z. Xue, G. Wang, J. Long, D. Kong, B. Liu, Z. Yang and D. Ding, *ACS Nano*, 2014, 8, 1475-1484.
4. B. V. Slaughter, S. S. Khurshid, O. Z. Fisher, A. Khademhosseini and N. A. Peppas, *Adv. Mater. (Weinheim, Ger.)*, 2009, 21, 3307-3329.
5. S. Van Vlierberghe, P. Dubruel and E. Schacht, *Biomacromolecules*, 2011, 12, 1387-1408.
6. E. F. Banwell, E. S. Abelardo, D. J. Adams, M. A. Birchall, A. Corrigan, A. M. Donald, M. Kirkland, L. C. Serpell, M. F. Butler and D. N. Woolfson, *Nat. Mater.*, 2009, 8, 596-600.
7. H. Wang, A. Han, Y. Cai, Y. Xie, H. Zhou, J. Long and Z. Yang, *Chem. Commun. (Cambridge, U. K.)*, 2013, 49, 7448-7450.
8. R. Ischakov, L. Adler-Abramovich, L. Buzhansky, T. Shekhter and E. Gazit, *Bioorg. Med. Chem.*, 2013, 21, 3517-3522.
9. J. Gao, W. Zheng, J. Zhang, D. Guan, Z. Yang, D. Kong and Q. Zhao, *Chem Commun (Camb)*, 2013, 49, 9173-9175.
10. J. Wang, Z. Wang, J. Gao, L. Wang, Z. Yang, D. Kong and Z. Yang, *J. Mater. Chem.*, 2009, 19, 7892-7896.
11. M. Ehrbar, R. Schoenmakers, E. H. Christen, M. Fussenegger and W. Weber, *Nat. Mater.*, 2008, 7, 800-804.
12. J. Nanda and A. Banerjee, *Soft Matter*, 2012, 8, 3380-3386.
13. H. Wang, Z. Yang and D. J. Adams, *Materials Today*, 2012, 15, 500-507.
14. A. N. Wilson and A. Guiseppi-Elie, *Adv Healthc Mater*, 2013, 2, 520-532.
15. C. A. Hauser and S. Zhang, *Chem. Soc. Rev.*, 2010, 39, 2780-2790.
16. L. Haines-Butterick, K. Rajagopal, M. Branco, D. Salick, R. Rughani, M. Pilarz, M. S. Lamm, D. J. Pochan and J. P. Schneider, *Proc. Natl. Acad. Sci. U. S. A.*, 2007, 104, 7791-7796.
17. S. Koutsopoulos and S. Zhang, *J Control Release*, 2012, 160, 451-458.
18. I. M. Geisler and J. P. Schneider, *Adv. Funct. Mater.*, 2012, 22, 529-537.
19. Y. Li, J. Rodrigues and H. Tomas, *Chem. Soc. Rev.*, 2012, 41, 2193-2221.
20. C. Yan, M. E. Mackay, K. Czymmek, R. P. Nagarkar, J. P. Schneider and D. J. Pochan, *Langmuir*, 2012, 28, 6076-6087.
21. C. Yan, A. Altunbas, T. Yucel, R. P. Nagarkar, J. P. Schneider and D. J. Pochan, *Soft Matter*, 2010, 6, 5143-5156.
22. E. L. Bakota, Y. Wang, F. R. Danesh and J. D. Hartgerink, *Biomacromolecules*, 2011, 12, 1651-1657.
23. M. C. Branco, D. J. Pochan, N. J. Wagner and J. P. Schneider, *Biomaterials*, 2010, 31, 9527-9534.
24. Y. Li, M. Qin, Y. Cao and W. Wang, *SCIENCE CHINA Physics, Mechanics & Astronomy*, 2014, 57, 849-858.
25. B. Ding, Y. Li, M. Qin, Y. Ding, Y. Cao and W. Wang, *Soft Matter*, 2013, 9, 4672-4680.
26. J. Wang, X. Miao, Q. Fengzhao, C. Ren, Z. Yang and L. Wang, *RSC Advances*, 2013, 3, 16739-16746.
27. Y. Li, Y. Ding, M. Qin, Y. Cao and W. Wang, *Chem. Commun. (Cambridge, U. K.)*, 2013, 49, 8653-8655.
28. J. Raeburn, A. Z. Cardoso and D. J. Adams, *Chem. Soc. Rev.*, 2013, 42, 5143-5156.
29. G. W. Ashley, J. Henise, R. Reid and D. V. Santi, *Proc. Natl. Acad. Sci. U. S. A.*, 2013, 110, 2318-2323.
30. N. S. Satarkar and J. Z. Hilt, *J Control Release*, 2008, 130, 246-251.
31. H. Epstein-Barash, G. Orbey, B. E. Polat, R. H. Ewoldt, J. Feshitan, R. Langer, M. A. Borden and D. S. Kohane, *Biomaterials*, 2010, 31, 5208-5217.
32. W. C. Jeong, S. H. Kim and S. M. Yang, *ACS Appl. Mater. Interfaces*, 2014, 6, 826-832.

33. M. Zhang, R. R. Parajuli, D. Mastrogiovanni, B. Dai, P. Lo, W. Cheung, R. Brukh, P. L. Chiu, T. Zhou, Z. Liu, E. Garfunkel and H. He, *Small*, 2010, 6, 1100-1107.
34. J. Liu, W. Yang, L. Tao, D. Li, C. Boyer and T. P. Davis, *J. Polym. Sci., Part A: Polym. Chem.*, 2010, 48, 425-433.
35. B. Adhikari, J. Nanda and A. Banerjee, *Chem.-Eur. J*, 2011, 17, 11488-11496.
36. J. M. Gosline, P. A. Guerette, C. S. Ortlepp and K. N. Savage, *J. Exp. Biol.*, 1999, 202, 3295-3303.
37. N. Du, X. Y. Liu, J. Narayanan, L. Li, M. L. Lim and D. Li, *Biophys. J.*, 2006, 91, 4528-4535.
38. C. M. Elvin, A. G. Carr, M. G. Huson, J. M. Maxwell, R. D. Pearson, T. Vuocolo, N. E. Liyou, D. C. Wong, D. J. Merritt and N. E. Dixon, *Nature*, 2005, 437, 999-1002.
39. Y. Ding, Y. Li, M. Qin, Y. Cao and W. Wang, *Langmuir*, 2013, 29, 13299-13306.
40. W. Li, J. Wang, J. Ren and X. Qu, *Adv. Mater. (Weinheim, Ger.)*, 2013, 25, 6737-6743.
41. K. Yang, S. Zhang, G. Zhang, X. Sun, S. T. Lee and Z. Liu, *Nano Lett.*, 2010, 10, 3318-3323.
42. C.-H. Zhu, Y. Lu, J. Peng, J.-F. Chen and S.-H. Yu, *Adv. Funct. Mater.*, 2012, 22, 4017-4022.
43. B. Adhikari, J. Nanda and A. Banerjee, *Soft Matter*, 2011, 7, 9259 - 9266.
44. J. Nanda, A. Biswas, B. Adhikari and A. Banerjee, *Angew. Chem. Int. Ed. Engl.*, 2013, 52, 5041-5045.
45. C.-a. Tao, J. Wang, S. Qin, Y. Lv, Y. Long, H. Zhu and Z. Jiang, *J. Mater. Chem.*, 2012, 22, 24856-24861.
46. C. Yan and D. J. Pochan, *Chem. Soc. Rev.*, 2010, 39, 3528-3540.

